JOURNAL OF SOLID STATE CHEMISTRY 116, 249–255 (1995)

On the Correlated Incorporation of Cu(II) Species in α- and β-$AlF_3 \cdot 3H_2O$: An ESR Study of Thermal Behavior

R. Stößer,[1] G. Scholz, and M. Päch

Institute of Chemistry, Humboldt University of Berlin, Hessische Strasse 1-2, D-10115 Berlin, Federal Republic of Germany

Received December 20, 1993; in revised form September 28, 1994; accepted October 3, 1994

A one-for-one substitution of Al^{3+} ions by Cu^{2+} ions in solids remains unknown thus far. Therefore, an incorporation of Cu^{2+} ions into α-$AlF_3 \cdot 3H_2O$ and β-$AlF_3 \cdot 3H_2O$ was attempted. ESR spectroscopic *in situ* investigations (X band) were carried out in the temperature range of 2 K $\leq T \leq$ 1073 K. The comparison of experimental with simulated ESR coupling tensors showed that both compounds allowed the incorporation of Cu^{2+} ions in a correlated manner. Depending on the reaction temperature, dimeric and monomeric species could be detected which provide the necessary compensation of charge and geometrical misfit. During thermal treatment, a superimposition of thermal and chemical processes takes place, assisted by the transition metal ions present.

INTRODUCTION

There is no report in the literature of a one-for-one substitution of Al^{3+} ions by Cu^{2+} ions in a well-ordered solid state. The reason for this seems to be the combined action of the required charge compensation and the often-observed effect that Cu^{2+} ions tend to make their own microenvironment. This is forced by the ground state configuration of the Cu^{2+} ions (^2D, $3d^9$) which includes the occurrence of the Jahn–Teller effect (1, 2). From the spectroscopic point of view, the paramagnetic probe reflects the local environment rather than the whole matrix.

In this work, an incorporation of Cu^{2+} ions into the two phases of aluminumfluoride trihydrate, α-$AlF_3 \cdot 3H_2O$ and β-$AlF_3 \cdot 3H_2O$, was attempted. Due to their flexibility, these two substances should in principle allow sufficient distortion to provide a place in the lattice for the Cu^{2+} ions. The aluminum atoms are surrounded by six ligands forming almost regular octahedra. Both α-$AlF_3 \cdot 3H_2O$ and β-$AlF_3 \cdot 3H_2O$ offer the possibility of a sixfold fluorine, oxygen, or mixed fluorine–oxygen coordination of the doping ions in the simplest case. Furthermore, the formation of other species such as aggregates or clusters should be taken into account. Even such aggregates should easily change their geometric and electronic structures to allow for the compensation of structural misfits.

The aim of this paper is to investigate what kind of Cu^{2+} species is formed during the incorporation into the above-mentioned aluminum trifluoride matrices, how the ions are included in the actual solid state, and how the local paramagnetic structure reacts formally to thermal perturbations. Furthermore, the question of whether the doping Cu^{2+} ions have an influence on the superimposed thermal and chemical processes should be answered. Generally, the ESR spectra of paramagnetic doping elements can make a unique contribution to the description of the process of thermal decomposition (3). Since Cu^{2+} ions exert a large influence on their surroundings, above a certain temperature range it can be expected that even a small concentration of these ions should be able to change the thermal properties of the whole matrix.

EXPERIMENTAL

Preparations

The preparations were made according to the method described in (4). Additionally, 10^{-3} mole $CuSO_4 \cdot 5H_2O$ per mole aluminum was added to the solution before precipitation.

ESR Measurements

The X-band ESR measurements were carried out with the help of the spectrometers E4 (Fa. Varian) and ESR 300 (Centre of Scientific Instruments, Berlin/Adlershof). The ESR measurements were performed in the temperature range 2 K $\leq T \leq$ 1073 K. For the calibration of the magnetic field, the B/NM2 magnetometer (Fa. Bruker, Karlsruhe) was used. A small sample of MgO/Cr^{3+} ($g' =$ 1.9796) served as a standard for the determination of g-values and line intensities. Measurements at low temperatures were performed with the He-Flow-Cryostat (Xtronics, Schweiz). For the high-temperature measurements, an HT high-temperature resonator (Fa. Bruker) was used. The Q-band measurements were taken at 298 K

[1] To whom correspondence should be addressed.

0022-4596/95 $6.00

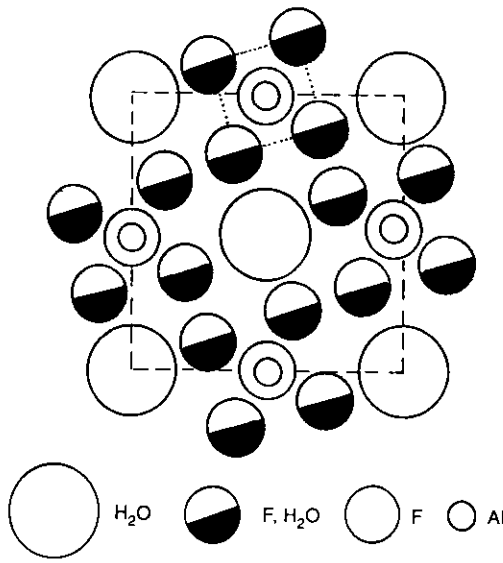

FIG. 1. Structure of β-$AlF_3 \cdot 3H_2O$ viewed along the c-axis.

on an ERS 220 spectrometer (Centre of Scientific Instruments, Berlin/Adlershof).

The simulations of the powder spectra with $S = 1/2$ and $S = 1$ were performed with a new program working on the basis of complete diagonalization of the spin-Hamiltonian matrix (5).

RESULTS AND DISCUSSION

Some Aspects of the Structure and Thermal Behavior of α-$AlF_3 \cdot 3H_2O$ and β-$AlF_3 \cdot 3H_2O$

For the presentation and discussion of the ESR results, a short overview of some known facts concerning the bulk properties of the matrices may be useful.

α-$AlF_3 \cdot 3H_2O$ has a rhombohedral structure, shows the effect of structural disorder at room temperature, and consists of a network of AlX_6 polyhedra (6, 7). The disordered structure implies that slightly distorted octahedra may be formed by an AlF_6^{3-}, $Al(H_2O)_6$, or mixed $[AlF_n(H_2O)_{6-n}]^{(3-n)}$ ($n = 0, \ldots, 6$) coordination. Figure 1 gives insight into the structure of β-$AlF_3 \cdot 3H_2O$ (8). In contrast to α-$AlF_3 \cdot 3H_2O$, the tetragonal structure contains chains of $[AlF_4(H_2O)_2]^-$ polyhedra along the c-axis. Adjacent octahedra share apices in the direction of the c-axis, and fluorine atoms are assumed to form these bridges between aluminum atoms. The four other components of each polyhedron are two fluorine atoms and two water molecules which are statistically distributed over these four positions. Additionally, water molecules are located in positions between the chains (Fig. 1).

From the thermal and X-ray analysis, both using α-$AlF_3 \cdot 3H_2O$ and β-$AlF_3 \cdot 3H_2O$ (*vide infra*), the following processes are recognized: (i) release of the largest amount of water up to 200°C; (ii) phase transition to β-AlF_3 (orthorhombic structure, see (9)), starting from α-$AlF_3 \cdot 3H_2O$, and to "γ-AlF_3" (cubic structure (10–12)) and traces of β-AlF_3, respectively, at temperatures $\geq$450°C, starting from β-$AlF_3 \cdot 3H_2O$; (iii) formation of the stable α-AlF_3 phase (for the structure, see (13)) at temperatures higher than 650°C.

ESR Results

The literature concerning the ESR of Cu^{2+} ions in fluoride compounds mainly deals with the spin-Hamiltonian parameters of the central ion itself (e.g., 14–16). Only a few papers are available which explicitly relate to bonding interactions between Cu^{2+} and F^- (e.g., 17–19). Unambiguous evidence for a Cu–^{19}F superhyperfine interaction is only given by a rare gas matrix ESR of, e.g., CuF_2 (20) and HCuF (21). Obviously, it is difficult to resolve this superhyperfine structure in condensed phases (2). This could be due to (i) its small value caused by the dominating ionic character of the Cu–F bonds and (ii) the dynamics of the fluorine bonds. Another difficulty originates from the incorporation of Cu^{2+} ions into the matrix of interest. As mentioned above, the Cu^{2+} ions tend to form their own local environment. The formation of clusters or autonomous phases would be an alternative. Such species, e.g., CuF_x or CuF_xO_y, were not detectable in the systems discussed here using X-ray diffraction methods. This does not, however, exclude their existence in an amorphous state.

The three-dimensional AlX_6 network of α-$AlF_3 \cdot 3H_2O$ is formed at room temperature. In contrast to the α-trihydrate phase, β-$AlF_3 \cdot 3H_2O$ is only formed if an excess of thermal energy is accessible. This favors the formation and incorporation of at least three different paramagnetic species. For both phases, the presence of water seems to be a necessity for the incorporation of Cu^{2+} ions into the lattices. In this connection, the question arises as to whether the geometrical structure of both phases forces the formation of certain CuF_xO_{6-x} ($x = 0, \ldots, 6$) polyhedra. The comparison with magnetic parameters of structures like CuF_2 or $CuF_2 \cdot 2H_2O$ (22) favors the assumption of the formation of this type of polyhedra. The ESR parameters of all experimental and simulated spectra are given in the captions of the figures.

α-$AlF_3 \cdot 3H_2O$

Figure 2 shows the ESR spectra at 298, 6, and 2.61 K. In this phase, Cu^{2+} ions form point defects with a well-resolved hfs and the nature and local geometry of elongated octahedra ($g_\parallel > g_\perp$). The second derivative of the $g_\perp$ region at 2.61 K (cf. Fig. 2e) yields more than eight hfs lines, a Cu–F coupling is indicated. The thermal treat-

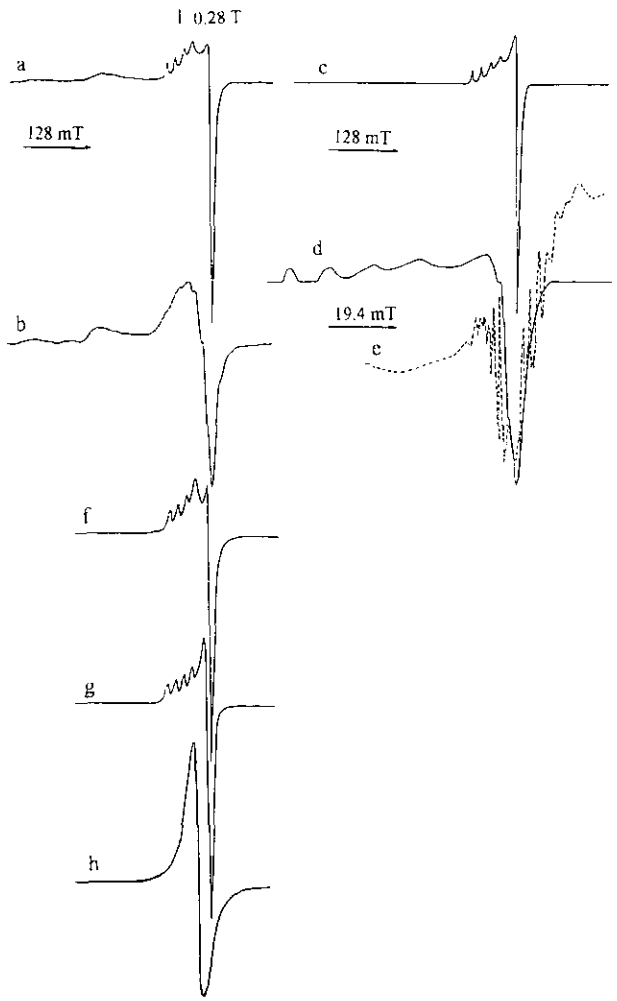

FIG. 2. ESR spectra of Cu^{2+} doped α-$AlF_3 \cdot 3H_2O$ at various temperatures ($c_{Cu^{2+}} < 10^{-3}$ mole): (a) 298 K; (b) external treatment, 4 hr, 500°C; (c) 6 K; (d) 2.61 K; (e) 2.61 K, second derivative in the $g_\perp$ range; expanded; (f) simulation of (a) as superimposition of (g) and (h); (g) simulation of the pure Cu^{2+} monomeric species: $g_\parallel = 2.4039$, $g_\perp = 2.0919$, $A_\parallel = 115$ G, $A_\perp = 24$ G, $\Delta B_i = 30$ G; and (h) simulation of a broad line at $g_i = 2.1959$, $\Delta B = 150$ G.

ment of the Cu^{2+} doped α-$AlF_3 \cdot 3H_2O$ phase does not result in the orthorhombic β-AlF_3 phase, as usually observed. An amorphous state was indicated by X-ray diffraction.

In the temperature range 2.6 K $\leq T \leq$ 300 K (cf. Fig. 2a–2d, 5a) only line-broadening effects could be observed. With increasing temperature ($T \geq 373$ K), the Cu^{2+} ions start to form species with stronger magnetic interactions, leading to a pronounced line broadening (Fig. 5a). After thermal treatment (4 hr, 500°C), the hyperfine structure disappears (see Fig. 2b). The temperature dependence of the ESR spectra and the corresponding simulations (cf. Fig. 2f–2h) give evidence that the experimental spectra represents a superimposition of different spectral contributions. As the simulation shows, the spectrum of Fig. 2a can be reproduced by an anisotropic part with $S = 1/2$ and an isotropic contribution (~40%) at $g' = 2.1959$. This effective g-factor together with the lineshape supports the assumption that the origin of this resonance lies in the interaction of Cu^{2+} ions via magnetic dipolar and exchange forces. This implies a nonuniform distribution of the Cu^{2+} ions with a finite probability of short copper–copper distances. Traces of $[Cu(H_2O)_6]^{2+}$, which also can contribute to the isotropic transition, cannot be completely excluded. One can assume that the contribution of the single line to the observed spectrum of the starting material will be enlarged with the temperature. The broad lines observed in the thermally treated α-$AlF_3 \cdot 3H_2O$/Cu^{2+} reflect the interactions mentioned above. Furthermore, there is also a correspondence to the broad-line spectra observed in the doped β-$AlF_3 \cdot 3H_2O$ at 200°C (Fig. 6a) (*vide infra*). There is no distinct microwave saturation of this broad line. This is caused by the spin–orbit coupling and the dipole–dipole interaction between the Cu^{2+} ions.

β-$AlF_3 \cdot 3H_2O$

The ESR spectra of the β-trihydrate phase at 298, 77, and 2.61 K are given in Fig. 3. Obviously, the doping proceeds by synchronous incorporation of different mono- and dimeric species (cf. Fig. 3); one of them shows a more pronounced saturation tendency. As Fig. 4a shows, the typical pattern of the mono- and dimeric species (cf. Fig. 3) including the distance between the main transitions of the $S = 1$ systems are conserved in the Q-band. By the effect of the g-values all Cu^{2+} signals are down-field shifted. The small Fe^{3+} impurities, present also in very pure AlF_3 samples, yield a signal at $g \sim 2$ which

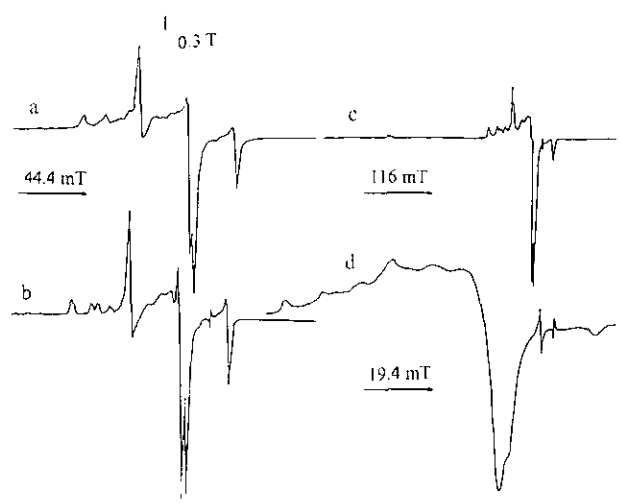

FIG. 3. Experimental ESR spectra of Cu^{2+} doped β-$AlF_3 \cdot 3H_2O$ (a) 298 K, 20 mW; (b) 77 K, 200 μW; (c) 2.61 K, 200 μW; and (d) 2.61 K, 20 mW.

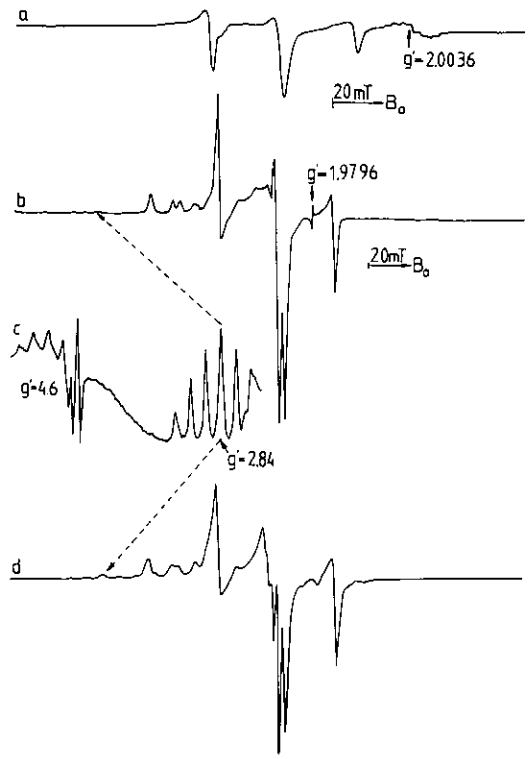

FIG. 4. ESR spectra of β-$AlF_3 \cdot 3H_2O$ doped with Cu^{2+} ions: (a) experimental spectrum measured in Q-band ($\nu \approx 34$ GHz) at 298 K; (b) experimental spectrum measured in X-band ($\nu \approx 9.2$ GHz) at 77 K; (c) low-field part of (b) expanded in the field scale and enlarged in amplitude; (d) simulation of (b) by superimposition of two monomeric (M_1, M_2) and one dimeric (Dim) species with the following parameters: M_1: $g_\parallel = 2.4069$, $g_\perp = 2.0829$, $A_\parallel = 112.8$ G, $A_\perp = 20.1$ G, relative intensity = 1.2; M_2: $g_\parallel = 2.3722$, $g_\perp = 2.0666$, $A_\parallel = 137.2$ G, $A_\perp = 20.1$ G, relative intensity = 1.0; Dim: $g_\parallel = 2.295$, $g_\perp = 2.0693$, $A_{\parallel/2} = 73.5$ G, $A_{\perp/2} = 10$ G, $|D| = 0.0548$ cm^{-1}, relative intensity = 0.1, $\Delta B_i = 30$ G.

shows a partially resolved superhyperfine structure of six nearly equivalent surrounding F^- ions. Under X-band conditions, the Fe^{3+} species contribute also at $g' \sim 2$ and obscure the $g_\perp$ signals of Cu^{2+}. Furthermore, small low-field peaks at $g' \sim 4.3$, 6, and 18 are caused by Fe^{3+} ions (not shown here).

Careful analysis of the low-field part of the spectrum depicted in Fig. 4b revealed not only the $\Delta m_s = 2$ transition at $g' \sim 4.6$ but also the Z_1 transition ($g' \sim 2.84$) of the dimeric species with $S = 1$ (Fig. 4c). Both the $\Delta m_s = 2$ and the Z_1 transition distinctly show the hyperfine splittings by two Cu nuclei with the half value of the coupling constant of the corresponding monomers. Together with the simulation, based on the parameters given in the legend of Fig. 4, the findings clearly indicate two monomeric and one dimeric Cu^{2+} species. The only assumption for this model was an exchange energy $E_{ex} \geq 15$ cm^{-1} (see also (23)).

Starting from the value of $D = 0.0548$ cm^{-1}, the distance between the two paramagnetic centers forming the $S = 1$ species was calculated to be 370 pm. A comparison with the Fe^{3+}–F–Fe^{3+} distance of ~387 pm in the structurally analogous and well-investigated β-$FeF_3 \cdot 3H_2O$ obtained from X-ray analysis (8) verifies that the distance of 370 pm should fit very well the Al^{3+}–F–Al^{3+} distance in β-$AlF_3 \cdot 3H_2O$. Therefore, the position of paramagnetic Cu^{2+} centers at Al^{3+} sites along the c-axis (Al–F–Al-direction) is suggested.

As known from other fluorine compounds containing copper (e.g. (24)), the formation of elongated $[Cu(H_2O)_4F_2]$ polyhedra is preferred for the first coordination sphere of Cu^{2+} ions. In principle, such polyhedra can be formed even within the chains along the c-axis of β-$AlF_3 \cdot 3H_2O$. But this circumstance would formally cause an excess of two F^- ions at Al^{3+} sites nearby and would need a charge-compensating process. For the latter, the incorporation of the dimeric Cu(II) species is proposed. Part of the charge compensation could also be achieved by local changes of the stoichiometry under participation of OH^- and other oxygen-related species. The two types of monomeric $S = 1/2$ Cu^{2+} systems are clearly observable only at low temperatures (e.g., 77 K). At room temperature (Fig. 3a), the differences are markedly reduced. Probably, the two types can represent, for example, a center of the same chemical nature forming differently distorted polyhedra as well as different linewidths (e.g., caused by surface effects). At 100°C, only one monomeric and one dimeric species could be observed. As for α-$AlF_3 \cdot 3H_2O$, a line broadening is also observed in the temperature range between 25 and 200°C for the β-trihydrate phase (cf. Fig. 5b). From thermal analysis it is known that the dehydration process is a continuous one, starting with rising temperature. The maximum water loss is in the region ~200°C. Because the shape of the ESR spectra shows no remarkable change of the local environment of the paramagnetic species up to 200°C, the dehydration process concerns water molecules originally located between the chains (cf. Fig. 1). The solid-state structure is reorganized at temperatures higher than 200°C. Consequently, the pattern of the discrete dimeric species with $|D| = 0.0548$ cm^{-1} disappears at 200°C and a broad line of magnetically stronger interacting Cu^{2+}–Cu^{2+} species appears. As the temperature exceeds 600°C, the spectra are dominated by exchange-coupled Cu–Cu species (cf. Fig. 6a). Additionally, the formation of FeF_6^{3-} takes place above 200°C.

Figure 6b shows the part of the Fe–^{19}F multiplet in the $g \sim 2$ region at 400°C, which exhibits only a small anisotropy. A line narrowing of the ^{19}F shfs caused by motional effects can be seen at temperatures higher than 600°C. From a theoretical point of view, the Δm_s $1/2 \Leftrightarrow -1/2$ transition of Fe^{3+} is only slightly dependent on the angle between the magnetic axis and B_0. This is the

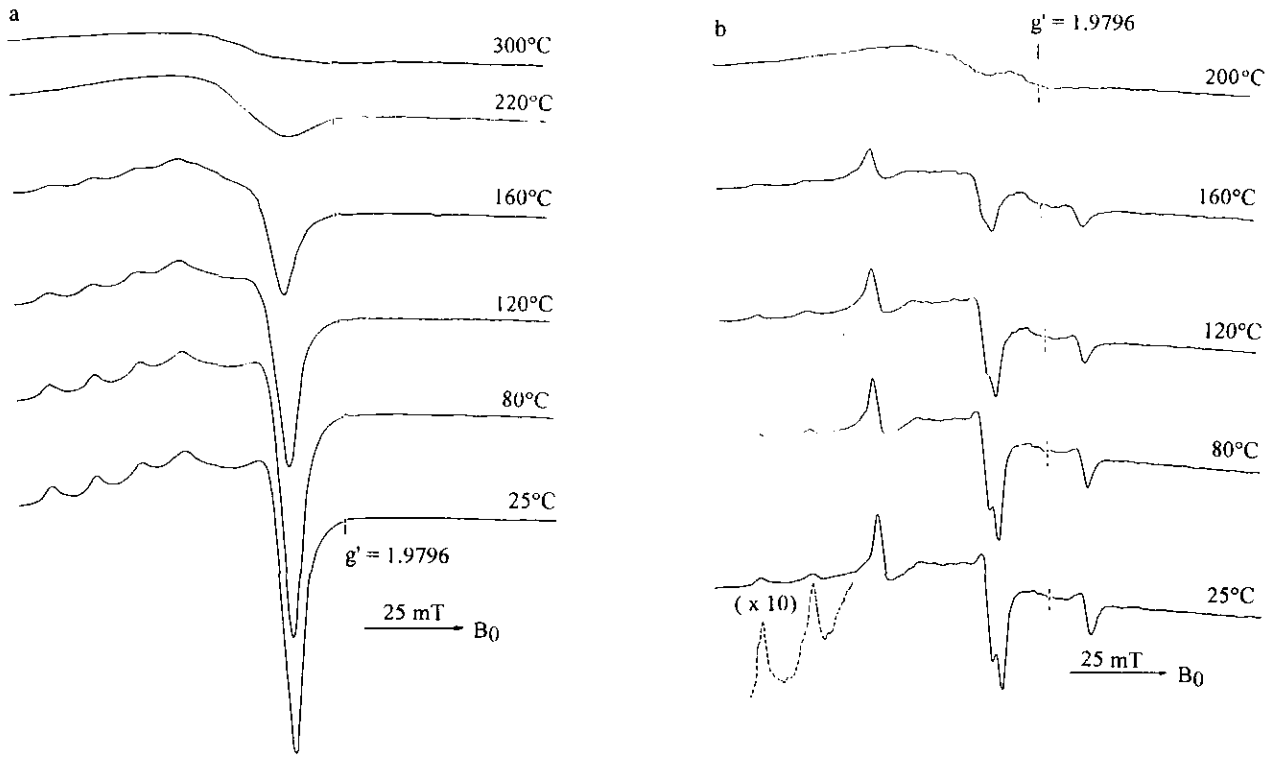

FIG. 5. Temperature dependence of the ESR spectra of (a) α-$AlF_3 \cdot 3H_2O$ doped with Cu^{2+} ions and (b) β-$AlF_3 \cdot 3H_2O$ doped with Cu^{2+} ions.

reason for a well-resolved shfs. Fe^{3+} ions are contained in the starting material and are probably bound as FeF_6^{3-} units on the surface of aluminumfluoride trihydrate. A portion of the trace Fe^{3+} can be a constituent of oxyhydrates localized at the surface too. As known for a variety of Fe^{3+} compounds, FeF_6^{3-} polyhedra are formed at a large F^- excess (25, 26). Therefore, any Fe^{3+} impurity will be transformed at higher temperatures into FeF_6^{3-} and incorporated as a spin probe substituting Al^{3+} ions in the lattice (see e.g. (3)). The formation of FeF_6^{3-} is favored above the temperature range studied for the α-phase in that paper. This is the reason for the absence of an FeF_6^{3-} signal in α-$AlF_3 \cdot 3H_2O$. As Figs. 6a and 6b show, this spin probe is sensitive to structural and dynamic changes in the system. This means that the anisotropy of the coupling tensors g and A depends on the structure of the matrix. The lattice dynamic is reflected by the motion-induced narrowing of the transitions of FeF_6^{3-}. Figure 6c depicts the saturation tendency of the FeF_6^{3-} multiplet at 200 mW which reflects the incorporation of Fe^{3+} into the lattice. Additionally, this figure shows the typical ESR spectrum of Cu species (like $[Cu(OH_2)_6]^{2+}$) or exchange-coupled species. This can be a consequence of the reaction of Cu^{2+} with water during the cooling process of the probe.

A comparison of the ESR spectra of an external and an *in situ* treatment of β-$AlF_3 \cdot 3H_2O$ (see Fig. 7) shows significant differences. The *in situ* measurement at 500°C (Fig. 7c) allows the detection of the well-resolved Fe–F superhyperfine structure of the Δm_s $1/2 \Leftrightarrow -1/2$ transition, narrowed by thermal stimulated motional effects. Furthermore, the lines of the Cu^{2+} species are broadened by the large and not completely averaged g and A anisotropies at higher temperatures. In contrast, after external treatment of heating in a furnace outside the spectrometer and measuring at 298 K in the spectrometer (Fig. 7a), the anisotropic Cu hfs is resolved and the Fe–F shfs is broadened by anisotropic contributions. In both cases, a Cu–F coupling could not explicitly be detected. Perhaps the formation of CuF_2 or CuF_xO_y phases is indicated.

CONCLUSIONS

As the ESR results presented here show, the structure of these types of aluminum fluorides is flexible enough to incorporate Cu^{2+} ions.But the most interesting fact is that the experimental conditions chosen here allow the doping of both Al^{3+} compounds, α- and β-$AlF_3 \cdot 3H_2O$, in a correlated manner: different monomeric and dimeric species are incorporated, and they provide the necessary compensation for charge and geometrical misfit caused by doping.

ESR spectroscopic *in situ* investigations (X-band)

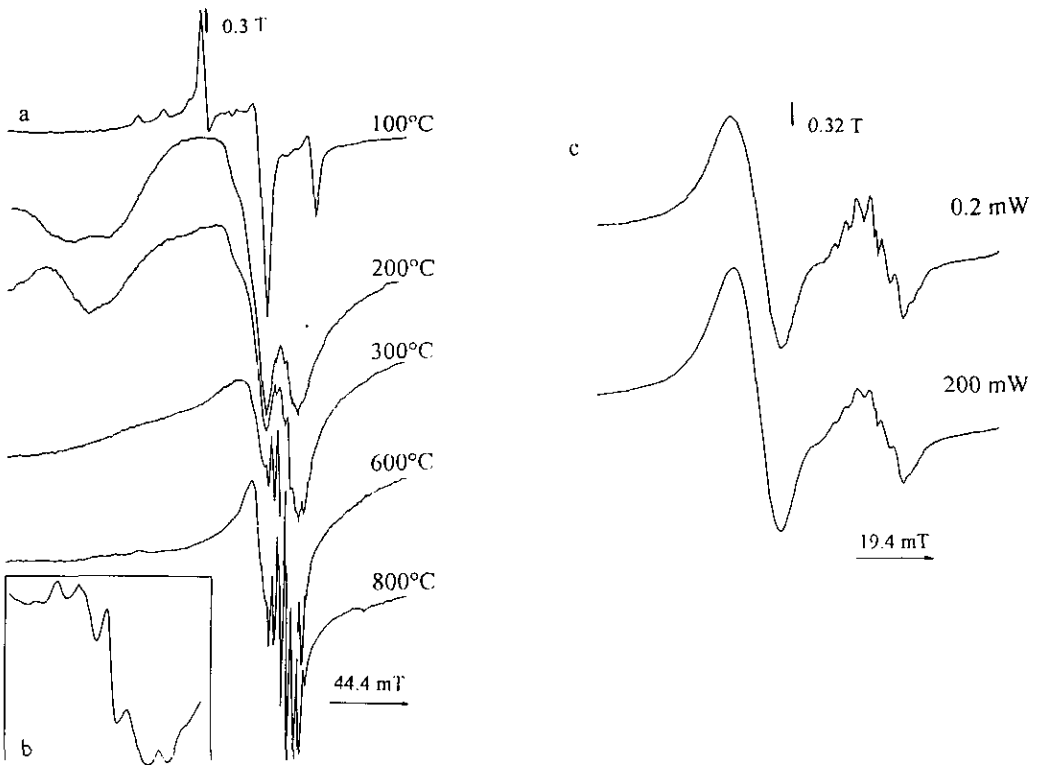

FIG. 6. ESR spectra of *in situ* thermal treatment of Cu^{2+} doped β-$AlF_3 \cdot 3H_2O$: (a) temperature range 100°C $\leq T \leq$ 800°C; (b) cutting out of the Fe–F multiplet at 400°C ($g \sim 2$); (c) dependence on the microwave power after 800°C *in situ* treatment, measured at 298 K.

were carried out in the temperature range 2 K $\leq T \leq$ 1073 K. The identification of coexisting paramagnetic Cu^{2+} species was possible by comparison of experimental with simulated ESR coupling tensors. In α-$AlF_3 \cdot 3H_2O$ the Cu^{2+} ions are incorporated in a monomeric form ($S = 1/2$, $I = 3/2$). The second derivative of the experimental spectrum at 2.61 K in the $g_\perp$ region indicates a Cu–F coupling. The doping of the β-phase of aluminumfluoride trihydrate requires at least the coexistence of three paramagnetic species: two different monomeric Cu^{2+} species, each with $S = 1/2$ and $I = 3/2$, and one dimeric species consisting of two coupled Cu^{2+} ions forming a triplet $S = 1$ state. The distance of 370 pm between the two Cu^{2+} centers determined from the zero-field splitting parameter D is compatible with the Al^{3+}–Al^{3+} distance in β-$AlF_3 \cdot 3H_2O$. This result and the microwave saturation effect at $T \leq 4$ K give evidence for the incorporation of the dimeric species in the lattice of β-$AlF_3 \cdot 3H_2O$. In the high-temperature region, some interesting effects can be observed: formation of Cu species, coupled by chemical bonds and magnetic dipolar and exchange interactions, and phase transitions accompanied by solid-state chemical reactions. Traces of Fe^{3+} species, present in the starting material, are converted into nonbridged FeF_6^{3-} polyhedra. Finally, the Cu^{2+} ions form magnetically strongly coupled aggregates.

In α-$AlF_3 \cdot 3H_2O$, the magnetic interaction between the Cu^{2+} ions, especially the exchange and dipolar ones, are more effective for the species characterized by an effective spin $S_{eff} \geq 1$. This means that a certain part of the $S = 1/2$ ions is coupled to an effective total spin which formally exceeds $S = 1/2$. They at least cause antiferromagnetic behavior.

In both α- and β-$AlF_3 \cdot 3H_2O$ the temperature dependence of the Cu^{2+} ESR spectra is in agreement with the findings of thermal methods (DTA-, TG-curves, see (10)).

From a catalytical point of view, it is interesting to note that during thermal treatment a superimposition of both thermal and chemical processes take place and are assisted by transition metal ions present ($T \geq$ 200°C). A consequence of this is the formation of a distorted but highly activated aluminum fluoride matrix which additionally contains unidentified amorphous products. It is interesting to note that, in contrast to the undoped material, a different thermal behavior results. No distinct phase transition was observable by thermal analysis, if the material was doped even with a very low concentration of Cu^{2+} ions (e.g., starting from 10^{-4} mole $CuSo_4 \cdot 5H_2O$ per mole aluminum).

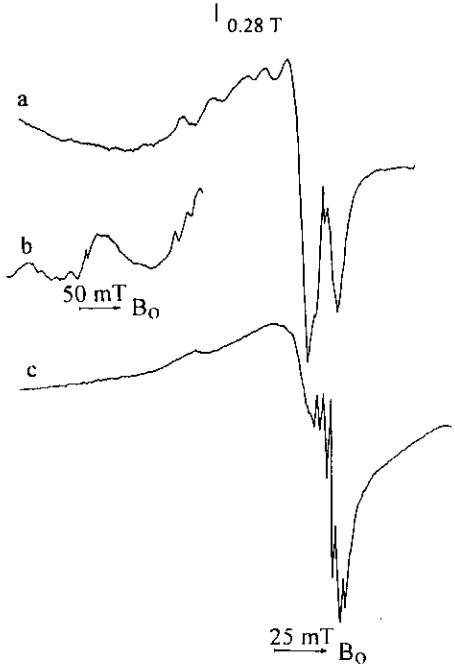

FIG. 7. Comparison of the ESR spectra of external and *in situ* thermal treatment of β-$AlF_3 \cdot 3H_2O$: (a) measured at 25°C, 4 hr, 500°C, external; (b) low field part of a; (c) 500°C *in situ*.

ACKNOWLEDGMENTS

We express our sincere thanks to Ms. I. Titt and Ms. W. Winkler for the preparation and external thermal treatment of the aluminumfluoride trihydrate samples and to Dr. D.-H. Menz for helpful discussions. The Deutsche Forschungsgemeinschaft is gratefully acknowledged for its financial support.

REFERENCES

1. I. B. Bersuker and V. Z. Polinger, "Vibronic interactions in molecules and crystals," Springer Series in Chem. Phys., Vol. **49**, Springer-Verlag, Berlin/Heidelberg, 1989.
2. D. Reinen and J.-M. Dance, *in* "Inorganic Solid Fluorides," p. 525. Academic Press, Orlando, 1985.
3. G. Scholz, R. Stößer, S. Sebastian, E. Kemnitz and J. Bartoll, *J. Phys. Chem. Sol.*, submitted.
4. A. Schmidt, *Monatsh. Chem.* **98,** 482 (1967).
5. N. Steinfeldt, R. Stößer, G. Scholz, M.v. Löwis, and A. Brückner, in preparation.
6. W. F. Ehret and F. J. Frere, *J. Am. Chem. Soc.* **67,** 64 (1945).
7. F. H. Herbstein, M. Kapon, and G. M. Reisner, *Z. Kristallogr.* **171,** 209 (1985).
8. G. Teufer, *Acta Crystallogr.* **17,** 1480 (1964).
9. A. Le Bail, C. Jakoboni, M. Leblanc, R. De Pape, H. Duroy, and J. L. Fourquet, *J. Solid State Chem.* **77,** 96 (1988).
10. D.-H. Menz, A. Zacharias, and L. Kolditz, *J. Therm. Anal.* **33,** 811 (1988).
11. Ph. Daniel, A. Bulou, M. Rousseau, J. Nouet, J. L. Fourquet, M. Leblanc, and R.Burriel, *J. Phys. Condens. Matter* **2,** 5663 (1990).
12. J. Ravez, A. Mogus-Milankovic, J. P. Chamuiade, and P. Hagenmuller, *Mater. Res. Bull.* **19,** 1311 (1984).
13. R. Hoppe and D. Kissel, *J. Fluorine Chem.* **24,** 327 (1984).
14. M. A. Hitchman, R. G. McDonald, and D. Reinen, *Inorg. Chem.* **25,** 519 (1986).
15. D. Reinen, M. Atanasov, G.St. Nikolov, and F. Steffens, *Inorg. Chem.* **27,** 1678 (1988).
16. C. Friebel, *Z. Naturforsch. B* **30,** 970 (1975).
17. T. C. Chiang and M. Bersohn, *Chem. Phys. Lett.* **1,** 521 (1968).
18. L. D. Bogomolova, E. G. Grechko, V. A. Yachkin, N. A. Krasilnikova, V. V. Sakharov, V. V. Sigaev, and S. I. Reinen, *Collect. Pap.-Int. Congr. Glass, 14th,* **1,** 178 (1986).
19. L. D. Bogomolova, V. A. Yachkin, N. A. Krasilnikova, V. L. Bogdanov, E. B. Fedorushkova, and V. D. Khalilev, *J. Non-Cryst. Solids,* **125,** 32 (1990).
20. P. H. Kasai, E. B. Whipple, and W. Weltner, Jr., *J. Chem. Phys.* **44,** 2581 (1966).
21. L. B. Knight, Jr., S. T. Cobranchi, B. W. Gregory, and G. I. Jones, Jr., *J.Chem. Phys.* **88,** 524 (1988).
22. A. F. Wells, "Structural Inorganic Chemistry." Oxford Univ. Press, Oxford, 1975.
23. J. R. Pilbrow, "Transition Ion Electron Paramagnetic Resonance." p. 351. Clarendon Press, Oxford, 1990.
24. S. I. Troyanov, I. V. Morozov, and Yu.M. Korenev, *Russ. J. Inorg. Chem. Engl. Transl.* **37,** 181 (1992).
25. R. Kalähne, E. Uhse, M.v. Löwis, R. Stößer, and D. Hass, *Z. Anorg. Allg. Chem.* **563,** 185 (1988).
26. E. Uhse, R. Stößer, D. Hass, and H. Mehner, *Z. Anorg. Allg. Chem.* **546,** 235 (1987).